Computing velocity models for S-wave static corrections using tau-differences in the rayparameter domain

Raul Cova, David Henley and Kris Innanen

ABSTRACT

A near-surface velocity model is one of the typical products generated when computing static corrections, particularly in the processing of PP data. Critically-refracted waves are the input usually needed for this process. In addition, for the converted PS mode, S-wave near-surface corrections must be applied at the receiver locations. In this case, however, critically-refracted S-waves are difficult to identify when using P-wave energy sources. Here we use the τ-p representation of the converted-wave data to capture intercept-time differences between receiver locations. These τ-differences are then used in the inversion of a near-surface S-wave velocity model. Our processing work-flow provides not only a set of raypath-dependent S-wave static corrections but also a velocity model that is based on those corrections. Our computed near-surface S-wave velocity model can be used for building migration velocity models or to initialize elastic full waveform inversions. Our tests on synthetic and field data provided superior results to those obtained by using a surface-consistent solution.

INTRODUCTION

The presence of poorly consolidated low velocity sediments in the near-surface can introduce significant delays in reflection traveltimes. These delays, often referred to as "statics", produce distortions in the moveout and structure of the seismic reflections. They also result in many cases in severe degradation of the resolution and stack power of the seismic events. Static corrections are usually derived from near-surface velocity and thickness information. In the processing of P-wave data some of this information is extracted from the analysis of critically-refracted P-waves.

Near-surface traveltime effects, both for P- and for S-waves, are commonly addressed by assuming surface consistency. Under this assumption, a single constant correction per trace removes the time delays introduced by the near-surface. The main assumption behind the idea of surface consistency is that a large velocity contrast exists between the low velocity sediments in the near-surface and the medium underneath. This results, according to Snell's law, in near-vertical raypaths through the near-surface layers. However, S-wave velocity gradients in the near surface can be lower than P-wave velocity gradients (Yilmaz, 2015). Therefore, the S-wave velocity contrast at the base of the sediments may not be large enough to support the vertical raypath assumption. The wider incidence angles needed to observe strong converted S-wave energy also threatens this assumption (Cox, 1999). Developments in multi-parameter full waveform inversion (FWI) also highlight the need for long-offset and wide-angle data to overcome model parameter crosstalk (Operto et al., 2013; Virieux and Operto, 2009). In this case, data preconditioning using surface-consistent corrections may not provide adequate results (Qu et al., 2017).

Due to the difficulty in computing S-wave velocity models for the near surface, S-wave

statics are usually computed by enhancing the coherency of PS events in common-receiver-stacked sections. Schafer (1991) presented a comparison of methods ranging from hand-picked statics on common-receiver stacks (Garotta and Granger, 1988), to those derived from Monte Carlo simulated annealing (Eaton et al., 1991). These methods offer a surface-consistent solution that provide adequate statics corrections for deep targets. However, shallow and wide angle data may require raypath dependent corrections (Cox, 1999).

Henley (2012) introduced a raypath-consistent approach in which no near-surface velocity model is needed. Instead, interferometric principles are employed to build a reference wavefield that is free of near-surface effects. Raypath consistency is achieved by processing the data in the radial-trace (RT) domain (Claerbout, 1983). Cova et al. (2017) extended this approach to the τ-p domain in which the kinematics of the raypath-dependency can honor vertical velocity changes.

Beginning with the kinematics presented by Cova et al. (2017), we have developed an inversion algorithm to compute near-surface velocity models from the raypath-dependent static corrections. In this way, we not only provide a set of S-wave statics corrections, but we are able to compute a near-surface S-wave velocity model related to them. This velocity information can be useful for converted-wave imaging and may provide an input into the creation of starting models for elastic FWI algorithms.

This report is divided into three sections. We first explain the mathematical framework that describes the kinematics of the raypath-dependency. Then, we compute synthetic converted-wave data and test the inversion. Finally, we test our method on a real converted-wave dataset from central Alberta, Canada.

RAYPATH-CONSISTENT NEAR-SURFACE CORRECTIONS

In a layered medium, the intercept time τ represents the aggregate product of vertical slownesses and thickness (Bessonova et al., 1974; Diebold and Stoffa, 1981; Hake, 1986):

$$\tau = \sum_{i=0}^{n-1} \Delta z_i \left(q_i^d + q_i^u\right) = \tau^d + \tau^u, \tag{1}$$

where q_i is the vertical slowness $q_i = \cos(\theta_i)/v_i$ in the i-th layer and Δz_i is the layer thickness $\Delta z_i = z_{i+1} - z_i$. The superscripts ^{d} and ^{u} denote the downgoing and upgoing legs of the raypath in Figure 1, respectively. For PS-waves the downgoing segments are controlled by P-wave velocities and the upgoing by S-wave velocities.

Assuming that the near-surface spans the first m layers and that the receiver lies in the $z_0 = 0$ plane, the upgoing τ-contribution in equation 1 can be rewritten as

$$\tau^u = \sum_{i=m}^{n-1} \Delta z_i q_i^u + z_m q_{m-1}^u + \sum_{i=0}^{m-1} z_{i+1} \left(q_i^u - q_{i+1}^u\right). \tag{2}$$

The first term in equation 2 gives the total upgoing τ-contribution from the conversion point to the base of the m-th layer. The second term represents the contribution from the

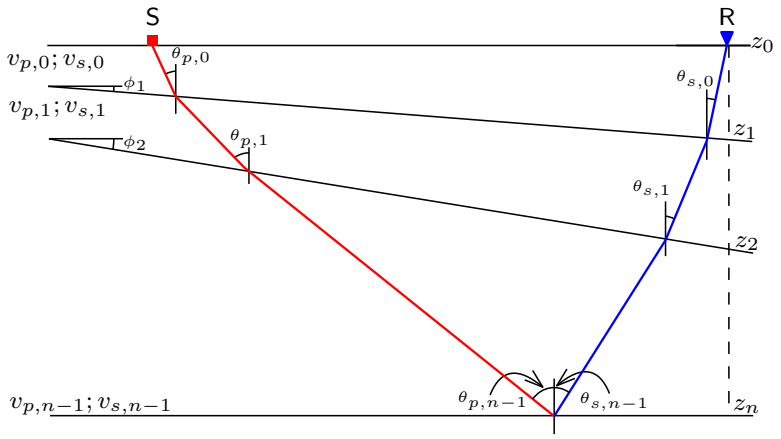

FIG. 1. PS raypath through a model with two dipping layers in the near-surface.

base of the m-th layer to the surface with vertical slowness $q_{m-1} = v_{m-1}/\theta_{m-1}$, as if the overlying m layers were not present in the model. This term accounts for the replacement process used in static corrections, with v_{m-1} being the equivalent to the replacement velocity and θ_{m-1} is here introduced as the replacement raypath angle.

The effect of the near-surface is therefore contained in the last term of equation 2. To remove the near-surface effect amounts to isolating and subtracting this term from the total intercept time. The receiver-side near-surface correction can then be written as

$$\Delta\tau^u = \sum_{i=0}^{m-1} z_{i+1}\left(q^u_{i+1} - q^u_i\right). \tag{3}$$

The correction shown in equation 3 represents a layer-stripping process in which the τ contribution of each layer i is subtracted and replaced by the τ contribution given by the propagation parameters in the underlying $(i+1)$ layer. Since the correction depends on the vertical slowness q of each layer, the raypath angles in each layer are honored.

The vertical slowness q is related to the horizontal slowness or rayparameter value p by the relationship $p^2 + q^2 = s^2$, where s is the total slowness or the velocity inverse $1/v$. In a horizontally layered media, according to Snell's law the rayparameter p is constant, even if conversion occurs along the ray. Hence, by knowing the rayparameter on the surface one can propagate this value through the subsurface if the geological conditions allow it. Therefore, the vertical slowness in each layer can be expressed as

$$q^u_i = \left(s_i^2 - p^2\right)^{1/2}. \tag{4}$$

Equations 3 and 4 are used as the engine for computing static corrections in the τ-p domain in a horizontally layered medium. Given the rayparameter values p measured at the surface, the velocities and thicknesses of the near-surface layers, one can compute the corrections needed to remove the effect of the near-surface in a raypath-consistent fashion.

Elevation corrections

Elevation or datum corrections are often handled by assuming vertical raypaths associated with the velocity of the replacement medium (Cox, 1999). For the sake of consistency we introduce a raypath-dependent elevation correction into our solution.

To extend the near-surface correction process up to a datum different from the recording surface an additional term in equation 3 is needed. This term can be written as,

$$\Delta\tau^u_{elev} = (z_d - z_r)\, q^u_{m-1}, \tag{5}$$

where z_d is the elevation of the final datum and z_r is the receiver elevation, measured from a fixed reference surface. Notice that for vertical raypaths, where $q = s$, equation 5 reduces to the most simple form of elevation correction $\Delta\tau^u_{elev} = (z_d - z_r)\,/v_{m-1}$.

Dipping near-surface layers

For dipping interfaces equation 1 still holds (Diebold and Stoffa, 1981). However, a dip correction is needed for each interface.

Two rotations can be used to address this problem. The first of them allows us to obtain the projection of the total slowness vector along the base of each near-surface layer. The apparent slowness p_a at the base of the m-th layer can be expressed as,

$$p_{a,m} = p\cos\phi_m - q_m \sin\phi_m. \tag{6}$$

According to Snell's law the tangential slowness must be preserved across interfaces. Therefore, the apparent perpendicular slowness on the $(m-1)$-th medium can be computed as

$$q_{a,m-1} = \left(s^2_{m-1} - p^2_{a,m}\right)^{1/2}. \tag{7}$$

However, these apparent slownesses are measured over the coordinate system defined by the dipping interface. To obtain the tangential and perpendicular slownesses as measured by the reference system defined by the recording surface one must apply a second rotation. This rotation can be written as,

$$\begin{pmatrix} p_{m-1} \\ q_{m-1} \end{pmatrix} = \begin{pmatrix} \cos\phi_m & \sin\phi_m \\ -\sin\phi_m & \cos\phi_m \end{pmatrix} \begin{pmatrix} p_{a,m-1} \\ q_{a,m-1} \end{pmatrix} \tag{8}$$

Equations 6 to 8 can be used to obtain the slownesses needed in equation 3 to compute the near-surface corrections. By including a dip correction, any asymmetry that may be present in the raypath dependent correction can be addressed (Cova et al., 2017).

Interferometric near-surface corrections in τ-p domain

Henley (2012) proposed an interferometric approach for near-surface corrections where time differences are captured by computing the crosscorrelation between raw traces and a

set of pilot traces. The latter are meant to approximate the recorded wavefield conditions as if the near-surface velocity anomalies had not been present. The same operation can be done in τ-p domain as shown by Cova et al. (2017). We propose using a fixed τ-p receiver gather, where the near-surface velocity model is assumed to be known as the representation of the reference wavefield. The τ-difference between the intercept-times at the j-th receiver location and the reference location j_0 is

$$\Delta\tau_{xcorr,j} = \tau_j - \tau_{j_0}. \tag{9}$$

Assuming that only the S-wave velocity structure of the first m layers in the near-surface has changed and including the elevation correction term (equation 5), we can write,

$$\Delta\tau_{xcorr,j} = \sum_{i=0}^{m-1} z_{i+1,j}\left(q^u_{i.j} - q^u_{i+1,j}\right) + (z_d - z_{r,j})\, q^u_{m-1} - \sum_{i=0}^{m-1} z_{i+1,j_0}\left(q^u_{i,j_0} - q^u_{i+1,j_0}\right) - (z_d - z_{r,j_0})\, q^u_{m-1}. \tag{10}$$

Reordering terms in equation 10, we obtain an expression for the τ-differences in terms of the near-surface corrections at the reference and current locations:

$$\Delta\tau_{xcorr,j} = \Delta\tau_{j_0} - \Delta\tau_j + (z_{r,j_0} - z_{r,j})\, q^u_{m-1}. \tag{11}$$

Therefore, if the near-surface parameters at a reference location are known, the near-surface corrections at a different location can be computed from the τ differences captured by the crosscorrelation. The last term in equation 11 allows us to include an elevation correction in the solution. In the next section we explain an iterative inversion scheme for computing the near-surface parameters.

INVERSION OF τ-DIFFERENCES

We employ a Gauss-Newton inversion approach to solve for the near-surface parameters. In this inversion an initial guess for the model parameters m is iteratively updated until the minimum of an objective function $\Phi(\mathrm{m})$ is reached. We used the L_2 norm of the data misfit (equation 12) as our objective function.

$$\Phi(\mathrm{m}) = ||\mathrm{g(m)} - \mathrm{d_{obs}}||^2, \tag{12}$$

where $\mathrm{d_{obs}}$ is the observed data and $\mathrm{g(m)}$ is the forward modelled data for a given set of model parameters m.

At the i-th iteration, the model parameters are updated as in equation 13.

$$\mathrm{m_i} = \mathrm{m_{i-1}} + \delta\mathrm{m_i}, \tag{13}$$

with the model update ($\delta\mathrm{m}$) given by equation 14.

$$\delta\mathrm{m_i} = \left[\mathrm{J(m_i)^T J(m_i)} + \mu\mathrm{I}\right]^{-1} \mathrm{J(m_i)^T}\delta\mathrm{d}, \tag{14}$$

where, μ is a regularization weight, I is the identity matrix, ($^{\mathrm{T}}$) denotes the transpose operator and $\mathrm{J(m)}$ is the Jacobian or sensitivity matrix.

In the case of a two-layer near-surface model there are six parameters to be solved for $(z_1, z_2, s_0, s_1, \phi_1, \phi_2)$. The associated sensitivity matrix is

$$\mathrm{J(m)} = \left[\frac{\partial \mathrm{g(m)}}{\partial \mathrm{z_1}}, \frac{\partial \mathrm{g(m)}}{\partial \mathrm{z_2}}, \frac{\partial \mathrm{g(m)}}{\partial \mathrm{s_0}}, \frac{\partial \mathrm{g(m)}}{\partial \mathrm{s_1}}, \frac{\partial \mathrm{g(m)}}{\partial \phi_1}, \frac{\partial \mathrm{g(m)}}{\partial \phi_2}\right]. \tag{15}$$

Using the formulae developed in the previous section, values for each of the derivatives in equation 15 can be determined. Expressions for each of these terms are presented in the following section.

Inversion sensitivities

The elements of the Jacobian matrix in equation 15 are obtained by taking partial derivatives of equation 11 with respect to each one of the model parameters. In the case of a two-layer velocity model the sensitivities related to the depth of each interface are

$$\frac{\partial \Delta\tau_{xcorr}}{\partial z_1} = q_1 - q_0, \tag{16}$$

$$\frac{\partial \Delta\tau_{xcorr}}{\partial z_2} = q_2 - q_1. \tag{17}$$

The derivatives with respect to the slownesses of the first two layers can be written as

$$\frac{\partial \Delta\tau_{xcorr}}{\partial s_0} = -\frac{z_1 s_0}{q_{a,0}}\cos(\phi_1), \tag{18}$$

$$\frac{\partial \Delta\tau_{xcorr}}{\partial s_1} = \frac{s_1}{q_{a,0}q_{a,1}}\left[(z_2 - z_1)q_{a,0}\cos(\phi_2) + z_1 p_0 \sin(\phi_2 - \phi_1)\right]. \tag{19}$$

Where

$$p_0 = q_{a,0}\sin(\phi_1) + p_{a,0}\cos(\phi_1), \tag{20}$$

and

$$p_{a,0} = p_1\cos(\phi_1) - q_1\sin(\phi_1). \tag{21}$$

Equations 20 and 21 represent the tangential slownesses measured along the surface and the base of the first layer respectively.

The sensitivity to changes in the dip of the first interface is given by

$$\frac{\partial \Delta\tau_{xcorr}}{\partial \phi_1} = \frac{z_1 p_0}{q_{a,0}}\left[q_{a,0} - p_1\sin(\phi_1) - q_1\cos(\phi_1)\right]. \tag{22}$$

Finally, we write the sensitivity to changes in the dip of the second interface in terms of the derivatives of the vertical slowness as

$$\frac{\partial \Delta\tau_{xcorr}}{\partial \phi_2} = (z_1 - z_2)\frac{\partial q_1}{\partial \phi_2} - z_1\frac{\partial q_0}{\partial \phi_2}, \tag{23}$$

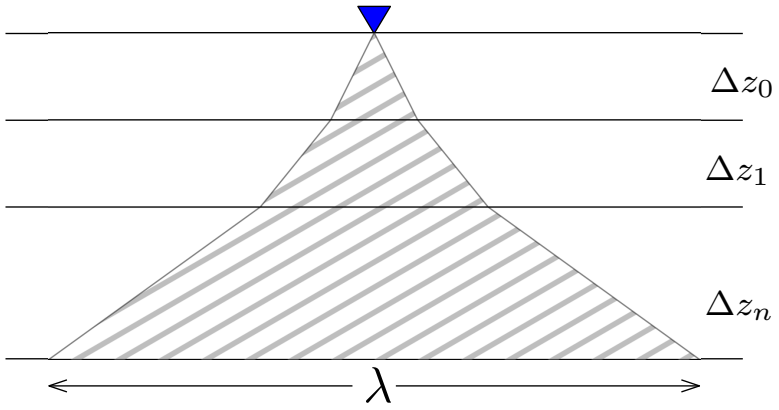

FIG. 2. Definition of the resolution limit (λ) below a receiver location. Model parameter variations within the grayed area will not be resolved in the inversion.

with

$$\frac{\partial q_1}{\partial \phi_2} = \frac{p_1}{q_{a,1}} \left[p \sin(\phi_2) + q_2 \cos(\phi_2) - q_{a,1} \right], \tag{24}$$

$$\frac{\partial q_0}{\partial \phi_2} = \frac{1}{q_{a,0} p_1} \left[q_1 \cos(\phi_1) - p_1 \sin(\phi_1) \right] \left[p_{a,0} \cos(\phi_1) - q_{a,0} \sin(\phi_1) \right] \frac{\partial q_1}{\partial \phi_2}. \tag{25}$$

The sensitivities for a one-layer model can be easily obtained by setting $z_2 = z_1$, $s_2 = s_1$ and $\phi_2 = \phi_1$. This will result in the vanishing of equations 17, 19 and 23.

Since the sensitivities to each extra layer depend on the parameters of the layers above we stop our derivation at the second layer. Including further layers in the model will increase the non-linearity of the problem, demanding a more complex inversion approach.

Lateral resolution

In spite of the assumption of a laterally homogeneous stratified medium, this condition is only required in the area covered by the range of raypath angles used for the inversion. Figure 2 illustrates this concept. Velocity variations withing the grayed area will not be acounted for in the inversion. Moreover, they can introduce short-wavelength near-surface effects that will not be resolved.

As illustrated in Figure 2, the lateral resolution of this method decreases with depth. We define the length (λ) measured at the base of the near-surface layers as the resolution limit of our approach. For a m-layered near-surface medium this can be computed as

$$\lambda_i = 2 p_{max} \sum_{i=0}^{m-1} \frac{\Delta z_i}{(s_i^2 - p_{max}^2)^{1/2}}, \tag{26}$$

where p_{max} is the absolute maximum rayparameter value measured at the surface. It is assumed that the range of p-values is symmetric ranging from $-p_{max}$ to p_{max}.

For a near-surface model of one layer with a velocity of 500 m/s, thickness of 100 m and a maximum rayparameter value of $1 \times 10^{-}3$ s/m, a lateral resolution of 115.5 m is

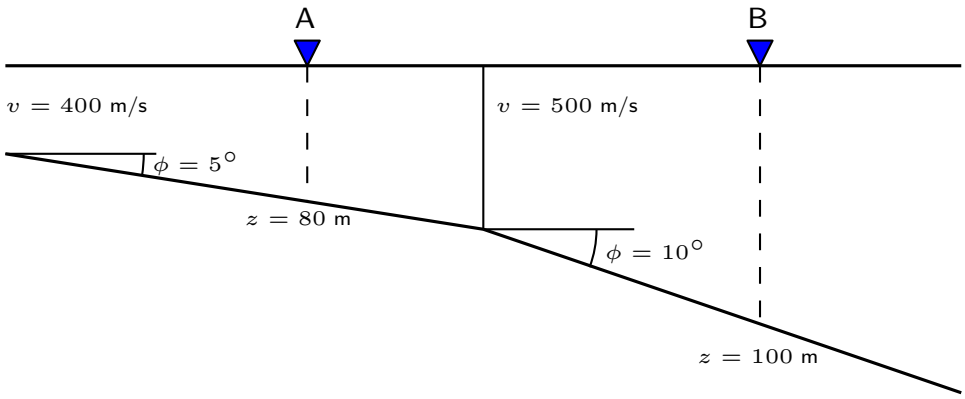

FIG. 3. Velocity model used for testing inversion sensitivities. Location A was used as the reference location were model parameter are assumed to be known. The goal of the inversion is to estimate the model parameters under location B.

obtained. The rayparameter value and velocity used in this example equates to scanning raypath angles from -30° to 30°.

Sensitivity to initial model parameters

Two models are required to initialize our inversion approach. First, model parameters are required to be known at a reference location. Secondly, an initial guess for the current location must be provided.

To test the sensitivity of the inversion to inaccuracies in the model parameters at the reference location we performed a series of inversion tests. Figure 3 shows a near-surface model with only one layer. Receiver location A is used as the reference location. We set the initial guess for the model parameters at B to be 20% larger than the true model parameters. We then performed the inversion using reference parameters with deviations between $\pm 30\%$ from the true values. Results are displayed in Figure 4a. There we can see how the error in the estimation of each model parameters varies depending on the accuracy of the model parameters for the reference location. Results show that the velocity of the near-surface is the most sensitive parameters to errors at the reference location. The error in the estimation of the velocity decreases as the reference parameters approach their true value. Estimations for the depth and dip of the near-surface layer are more stable, particularly when the reference parameters are underestimated. The error in the dip estimations increases significantly as the reference parameters are overestimated.

We then performed a series of inversions using the true parameters at the reference location but with different initial parameters for the location B. The results on Figure 4b show that model parameters were inverted with errors of less than 0.12% when the initial guess ranged between $\pm 30\%$ of their true values.

Similar tests were performed with the two-layer velocity model sketched in Figure 5. The results on Figure 6a show that the errors in the estimations are more stable when model parameters are underestimated. The dip of both layers and the velocity of the first layer are the most sensitive parameters to errors in the reference parameters. In contrast,

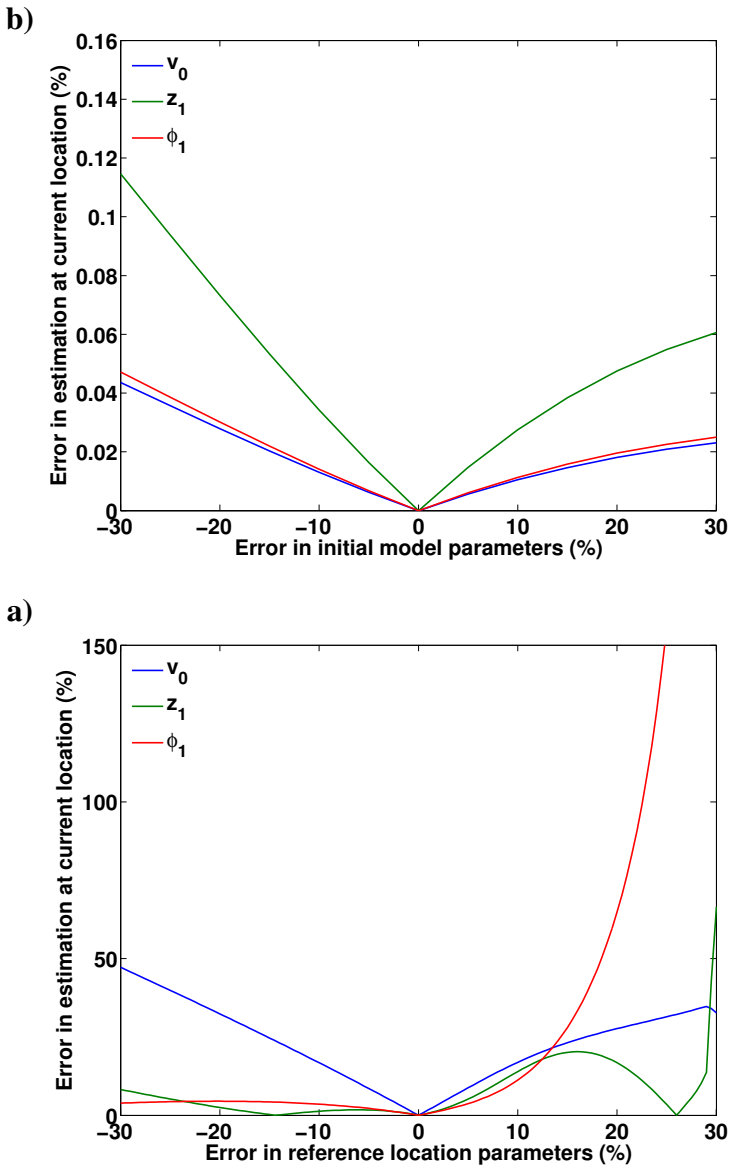

FIG. 4. (a) Errors in the estimation of model parameters for a range of reference parameters between $\pm 30\%$ of the true model parameters at the reference location. (b) Errors in the estimation of model parameters for a range of initial models between $\pm 30\%$ of the true model parameters under location B.

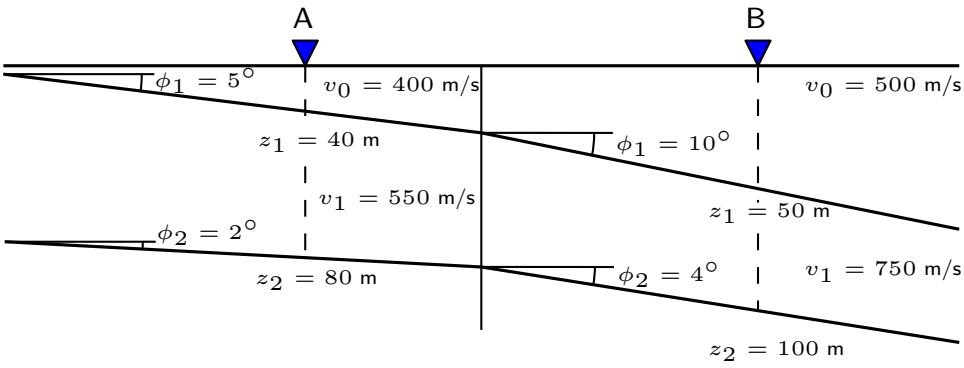

FIG. 5. Two-layer model used for testing inversion sensitivities.

the depth of both layers and the velocity of the second layer are less affected by errors in the reference parameters. Estimations for all parameters become highly unstable as the reference parameters are overestimated. These instabilities could be related to singularities in the sensitivities respect to each model parameter.

Figure 6b shows that the errors in the inversion of all parameters remained very stable, particularly when the initial guess for each model parameter presented between -30% and 25% of error respect to the true values. Errors in the inversion increase significantly when the initial parameters are overestimated by more than 25%.

SYNTHETIC DATA ANALYSIS

To examine the behavior of the inversion algorithm developed in the previous section, we computed PS converted-wave synthetic traces via raytracing using the velocity model illustrated in Figure 7. Notice that no P-wave velocity contrast exists between the near-surface layer and the medium beneath. This simulates the case where P-wave statics have already been removed. The S-wave velocity model consists of two near-surface layers with velocities of 450 m/s and 600 m/s, respectively. A channel-like anomaly is included on the right hand side of the model.

The effect of the near-surface structure on the travel times is evident on the source gather shown in Figure 8a. This gather corresponds to the data recorded from a source located at location B in Figure 7. The moveout of the converted-wave traveltimes has been clearly deformed by the presence of low S-wave velocities in the near-surface. In contrast, the receiver gather recorded by a receiver at location B (Figure 8b), displays a more coherent moveout. Since there are no near-surface P-wave velocity changes, only P-wave elevation statics were used on the source side.

Even though S-wave near-surface effects are not evident on receiver gathers they are highlighted when comparing gathers from different locations. We do such comparison after transforming the data to the τ-p domain. Figure 9 displays two receiver gathers, corresponding to locations A and B in Figure 7, after transformation to the τ-p domain. The third panel to the right shows the output crosscorrelation functions and the picks at the maximum value of the functions. Notice that these picks match closely the modelled τ-differences predicted by equation 11. The two gaps around p=0 s/m and 0.19×10^{-3} s/m

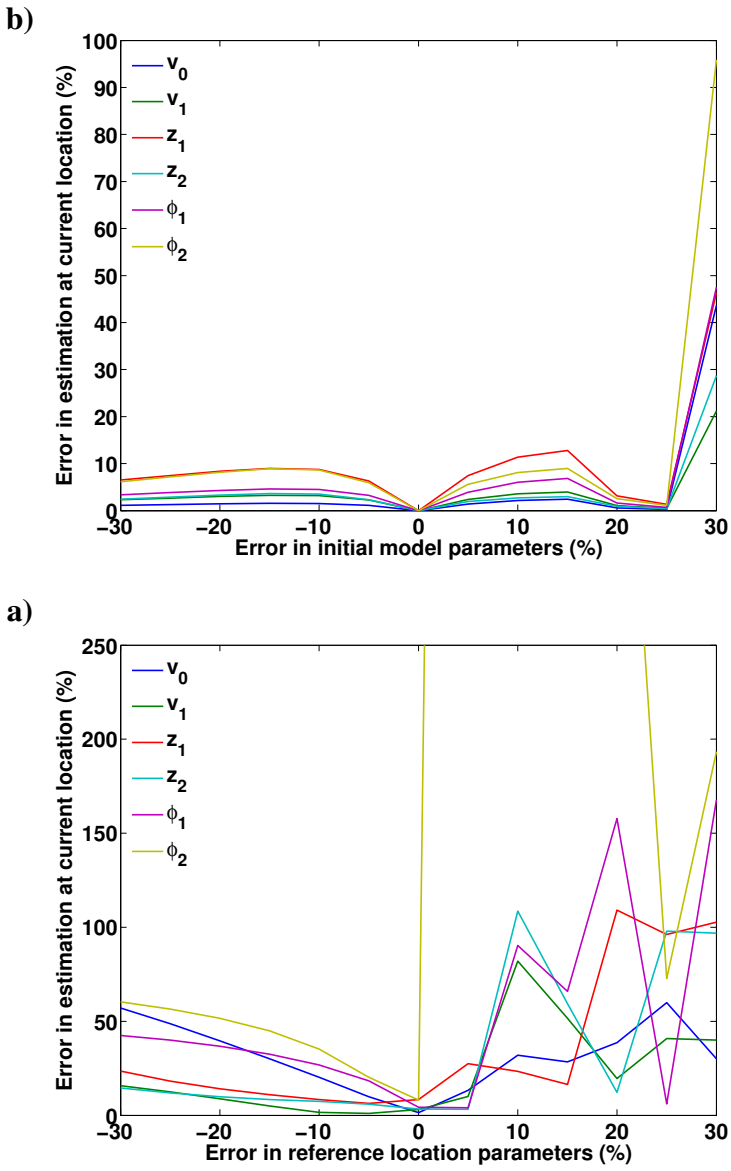

FIG. 6. (a) Errors in the estimation of model parameters for a range of reference parameters between $\pm 30\%$ of the true model parameters at the reference location. (b) Errors in the estimation of model parameters for a range of initial models between $\pm 30\%$ of the true model parameters under location B.

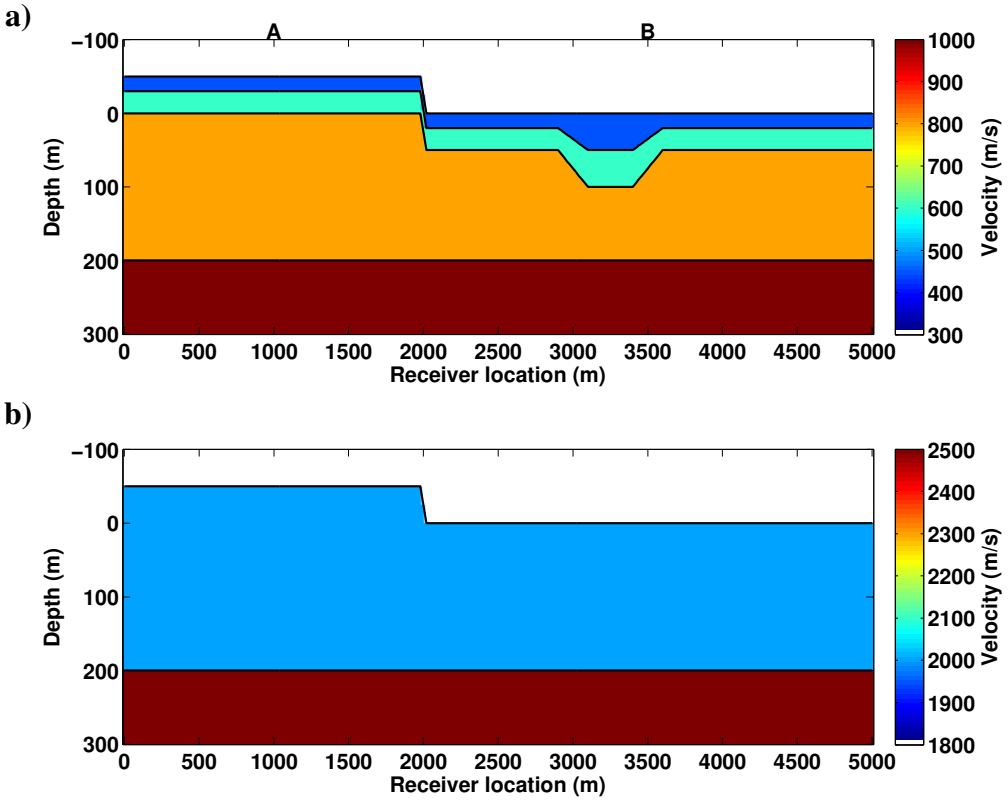

FIG. 7. (a) S-wave and (b) P-wave velocity models used for raytracing PS-data. No near-surface velocity changes exist on the P-wave velocity model to simulate the case where P-wave near-surface effects have been already removed. Only P-wave elevation corrections are needed on the source side for this case.

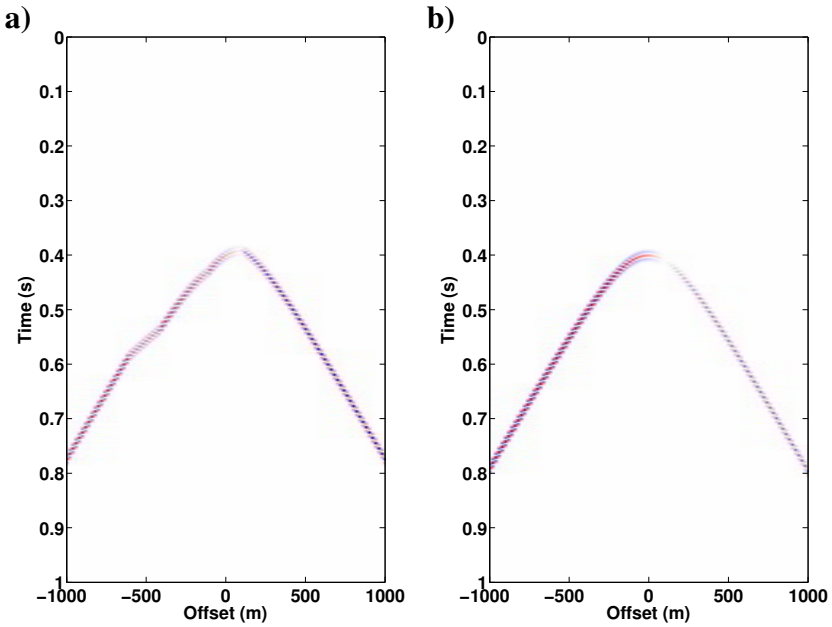

FIG. 8. (a) Source and (b) receiver gathers obtained at location B in Figure 7. The imprint of the structure of the near-surface layers is very clear on the source gather (a). Since source-side elevation statics have been applied and no P-wave near-surface effects were modeled, the moveout of the event in the receiver gather (b) displays no deformation.

are a results of the polarity reversals shown in Figure 8. Since the near-surface structure beneath the receiver location B is dipping, the location of this polarity reversal is shifted toward positive offsets. Polarity reversals should be addressed before τ-p transformation to avoid the presence of artifacts in the output.

Gaussian pseudo-random noise with zero mean and a standard deviation of 4 ms was added to the $\Delta\tau$-picks to simulate pick errors. Figure 10 shows the inversion results in the data domain. We assumed that model parameters for location B to be equal to those in location A. Therefore, the initial guess of the τ-differences between these two locations are zero. The stop criterion for the inversion code was the number of iterations. Inspection of the evolution of the objective function values allowed us to inspect that the number of iterations was enough to ensure convergence toward a stable solution. In this case, after fifteen iterations the inversion converged to a solution very close to the actual model parameters. Data residuals dropped from 18.7 ms to 4.3 ms, slightly above the noise level. The depth of each near-surface layer were estimated at 40.8 m and 65.4 m respectively. This represent an error of 5.8 m (12.4%) and -9.58 m (-17.2%) in the z_1 and z_2 estimations, respectively. Since we used location A as a fixed reference location, any errors in the picks at this location will be propagated to the rest of the model.

This process is repeated for all receiver locations to invert for the near-surface structure. In Figure 11 the inverted S-wave velocity model for the near-surface is plotted. The dashed lines represent the actual depths of the two interfaces defined in the original model. In the area nearby the channel-like feature, the average absolute errors for the depths of the first and second interfaces were 8.4 m (16.8%) and 14.6 m (14.6%), respectively. Outside of that

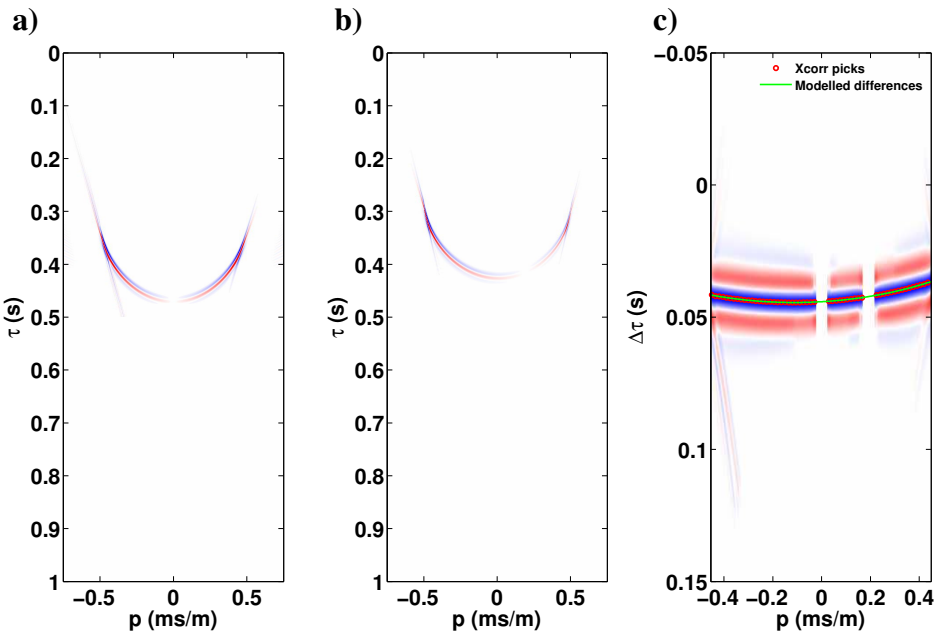

FIG. 9. τ-p receiver gathers obtained at locations (a) A and (b) B in Figure 7. (c) Crosscorrelation between (a) and (b). The maximum of the crosscorrelation functions matches the τ-differences given by equation 11.

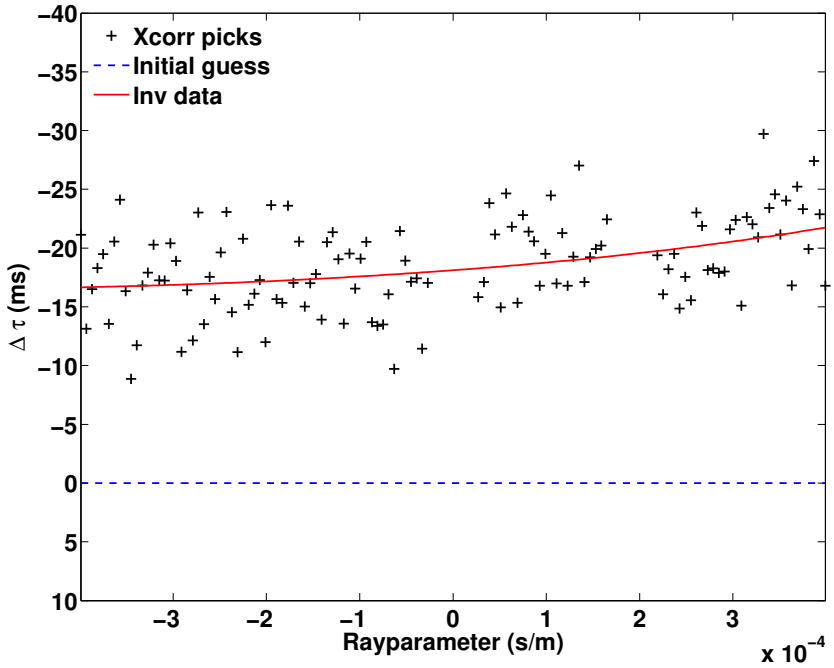

FIG. 10. Inversion results obtained from the τ-differences captured in Figure 9c. The same parameters assumed to be known at location A were used as the initial guess for the parameters at location B. For this reason the initial model differences are zero. After 10 iterations the inverted differences model the picked differences providing an estimation of the near-surface parameters at location B.

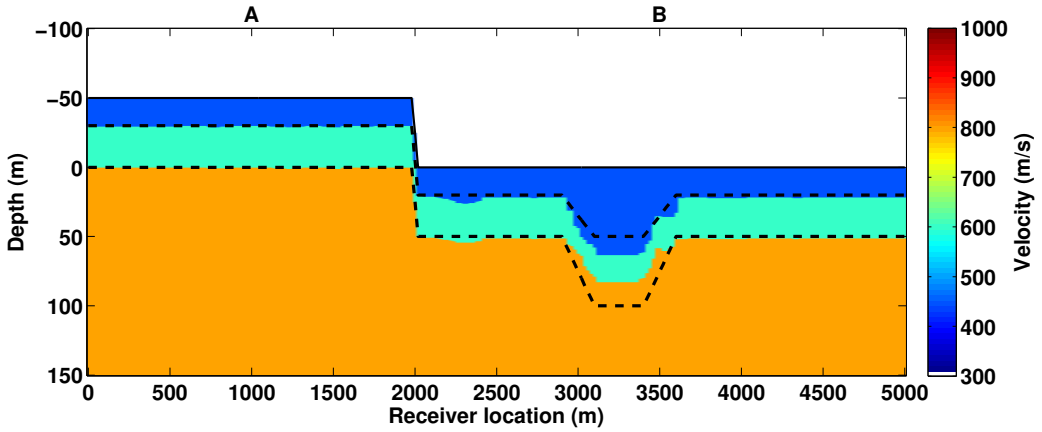

FIG. 11. Near-surface S-wave velocity model inverted from the synthetic data. The dashed lines represent the actual depth of each velocity change. The average absolute errors are of 2.42 m and 3.52 m for the depth estimations and, 0.76 m/s and 5.2 m/s for the velocity estimations of the first and second layer, respectively.

area the errors drop to 0.9 m (4.5%) and 0.6 m (1.2%), respectively. Velocity estimation was stable along the model with average absolute errors of 0.1 m/s (0.02%) and 0.2 m/s (0.03%) for the first and second layers, respectively.

These synthetic data results illustrate the process of using the τ-differences captured by the crosscorrelation functions to obtain a S-wave velocity model for the near surface. In the next section we apply this processing to a field dataset.

FIELD DATA EXAMPLE

The field data used in this part of the study were acquired by the Consortium for Research in Elastic Waves Exploration Seismology (CREWES) in the Hussar area in Southern Alberta (Margrave et al., 2012). The seismic survey consisted of a multicomponent 2D line with sources and receivers spaced every 20 m and 10 m, respectively, over a length of 4.5 Km. Source-side statics were computed using the first arrivals recorded in the vertical component data and surface-wave data were removed from all the components using a velocity filter. In Figure 12 a common receiver stacked section using the radial (PS) component data is plotted. There, near-surface/elevation effects are evident. Particularly, in the vicinity of the receivers located between 1750 m and 2250 m along the line, all events display an important pull-down of about 100 ms. Many small-scale undulations are also observed along the rest of the line. The vertical (PP) component sections processed in this area display very continuous and coherent horizontal events (Henley, 2014).

Figures 13a and 13b display two different receiver gathers after surface-wave removal and P-wave static correction. These receiver gathers correspond to locations A and B in Figure 12, respectively. The transformation of these gathers to the τ-p domain is plotted in Figures 13c and 13d. The τ-differences between the data recorded at these two receiver locations is captured by the crosscorrelation operation (Figure 13e).

The τ-lags associated with the maxima of the crosscorrelation functions are then extracted and input into the inversion scheme outlined previously. Figure 14 displays the

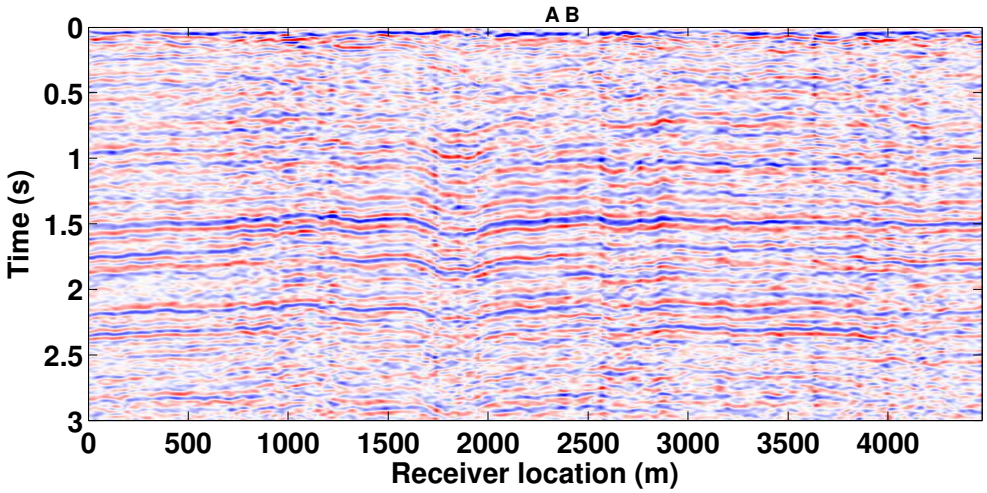

FIG. 12. Common-receiver stacked section for the Hussar dataset. Only source side statics were applied at this stage. Notice the pull down of the events particularly on the traces around 1750 m along the line. Shorter wavelength undulations are also observed along the section.

input and predicted data from the inverted model for this case. Only the absolute rayparameter values between 0.5×10^{-4} s/m and 3×10^{-4} s/m were used in the inversion. Within this range most of the crosscorrelation functions show significant energy. We chose not to include picks from rayparameter values lower than 0.5×10^{-4} s/m given that PS reflectivity is expected to be very low as the normal incidence condition is approached. The large crosscorrelation energy around $p = 0$ s/m could be the result of coherent noise still present in the data.

The near-surface parameters for the reference location A were taken from a previous surface-wave velocity inversion study done with the same data (Askari et al., 2012). A two layer velocity model was assumed with $z_1 = 40$ m, $z_2 = 100$ m, $v_0 = 400$ m/s, $v_1 = 600$ m/s. The replacement velocity was set at 800 m/s. Since the maximum surface elevation is 983.4 m we set the final datum at 990 m. As the initial guess for the receiver location B we used the same parameters used for location A. For this reason the τ differences modeled with the initial parameters are zeros. The inverted model for the receiver location B provided $z_1 = 43.2$ m, $z_2 = 101.7$ m, $v_0 = 390.2$ m/s and $v_1 = 568.6$ m/s, with an average misfit of 4.1 ms on the data domain.

The undulations on the picks on Figure 14 might be the result of short-wavelength near-surface effects might still present in the data. These variations could be the result of fast lateral velocity changes within the near-surface that are not accounted for in our method.

In Figure 15 the inverted velocity model and the average relative misfit obtained at each receiver location are plotted. The largest velocity changes in the model are located nearby the topographic high located around 1750 m. This anomaly appears to be the cause of the pull down observed on the initial common-receiver stack (Figure 12). The relative average

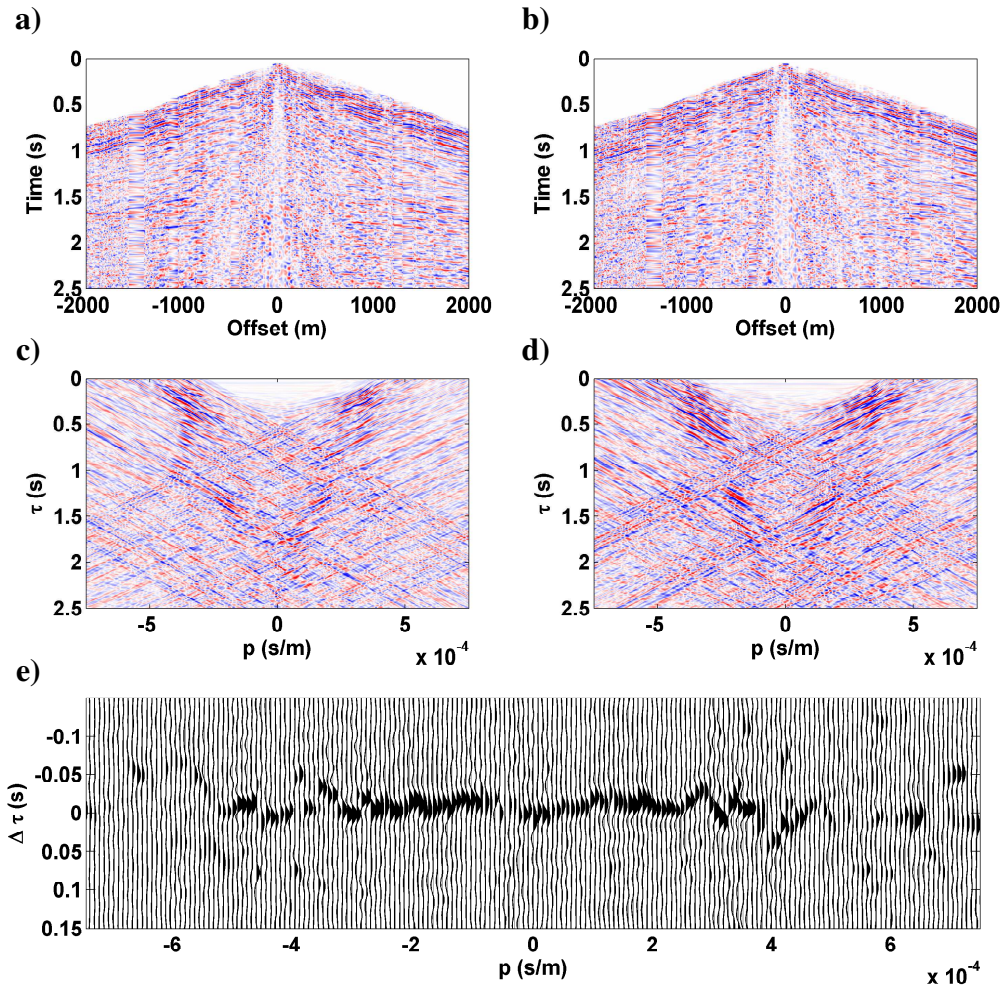

FIG. 13. Receiver gathers recorded at the positions (a) A and (b) B in Figure 12 and their τ-p representations (c) and (d), respectively. (e) Crosscorrelation between (c) and (d). Notice that the crosscorrelation functions display significant energy for absolute rayparameter values smaller than 3×10^{-4} s/m.

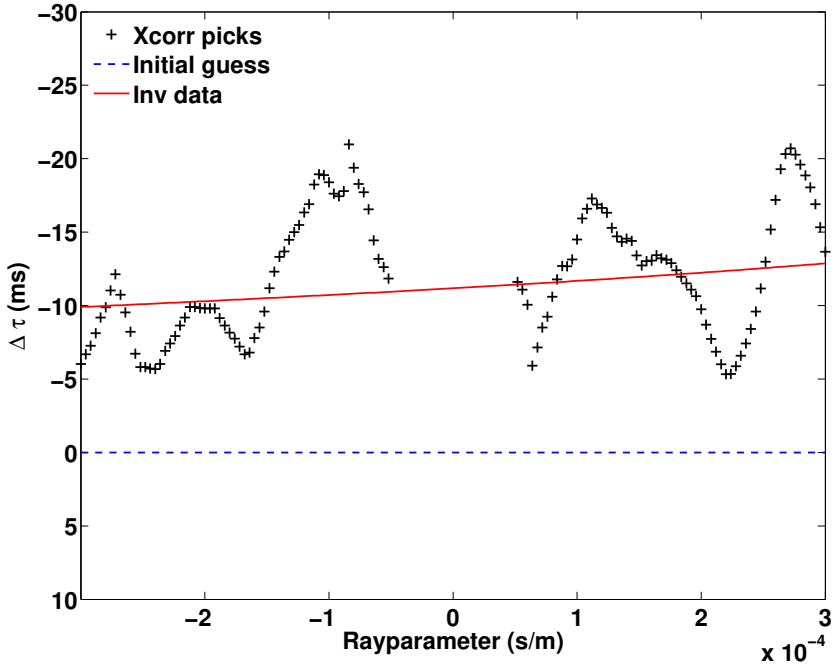

FIG. 14. Data domain inversion results. Only τ-differences between 3×10^{-4} s/m and 0.5×10^{-4} s/m were used for the inversion. The average misfit between the final modeled data and the input data is 4.1 ms.

misfit along the section was 0.51, decreasing to about 0.11 for the receivers closer to the reference location. According to these results the data computed using the inverted velocity model differs by 51% from the measured data. Receiver locations with large relative misfit values (~ 1) displayed very low signal-to-noise ratio and low crosscorrelation energy. The misfit increases toward the end of the lines as a result of fewer rayparameter values available for the inversion.

The rayparameter-dependent static corrections computed from this model are plotted in Figure 16. The correction due to elevation changes is displayed on Figure 16a and the component due to near-surface variations is displayed on Figure 16b. Both corrections display similar absolute magnitude ranges for this dataset. Elevation corrections range between -50 ms and -110 ms while near-surface corrections range between 10 ms and 110 ms. The total static corrections displayed on Figure 16c are indicative of a negative correction (~ -25 ms) around 1750 m that should remove the pull down present in the common receiver stack. This range of values contrasts with the results reported by Askari et al. (2012) where static corrections between 20 and -10 ms were obtained. The investigation depth of their MASW velocity model was of maximum 50 m. These two observations motivated our claim that static corrections computed from MASW velocity models may underestimate the near-surface effects.

After applying the trace shifts displayed in Figure 16c to the τ-p receiver gathers, the data were transformed back to the x-t domain. The new common receiver stack is displayed in Figure 17. Notice how all deformations present in Figure 12 have been removed. Especially for times earlier than 1 s, more events are now visible and the data display an

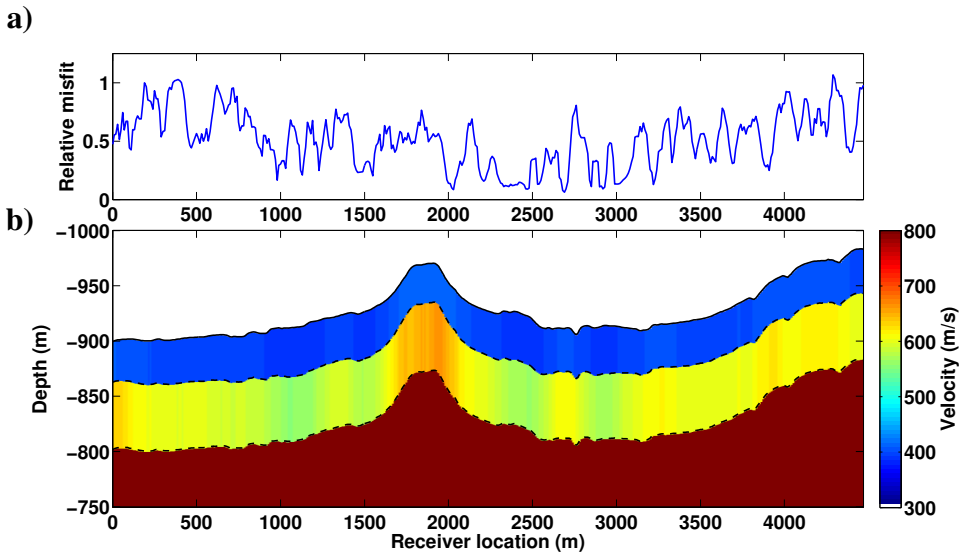

FIG. 15. (a) Relative inversion misfit (ratio between the average misfit and the average measured $\Delta\tau$) per receiver location, and (b) inverted near-surface S-wave velocity model for the field data. The average misfit is 0.51, which indicates that the inverted model explains about 51% of the data. Misfit values increase toward the end of the line as a result of having fewer rayparameter values available for the inversion.

improved coherence.

For comparison, a common receiver stack obtained using a surface-consistent solution, which is standard processing, is displayed in Figure 18. There, events shallower than 1 s show significantly lower degree of continuity. Moreover, the overall coherency of the events in the section is lower than in Figure 17.

CONCLUSIONS

Removing near-surface effects in a raypath-consistent framework provides stacked sections with enhanced coherence and resolution. Our approach removes raypath-dependent near-surface effects while simultaneously extracting information about the velocities in the near-surface. In this way, the corrections applied to the data can be removed at later stages of the processing if needed. Also, the velocity information about the near-surface layers can be useful for building velocity models for migration or elastic full waveform inversion.

The raypath-dependent solution presented here assumes a stratified near-surface. As in the MASW method the velocity model here obtained is constructed from several 1D inversions that are merged assuming smooth velocity changes between measurement locations. As a result, this approach may be counter-indicated in areas with structurally complex near-surface conditions.

A single reference location was used in our inversion constraining the results to solutions close to the model parameters affecting the reference location. This setup provided

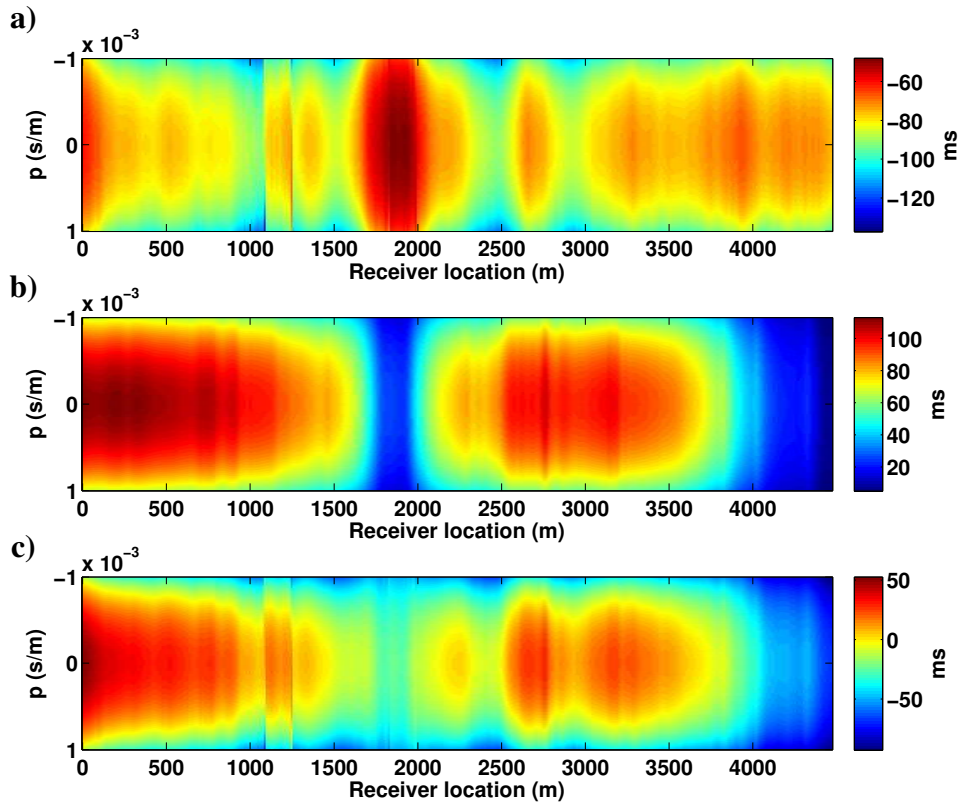

FIG. 16. Rayparameter dependent corrections: (a) elevation, (b) near-surface and (c) total corrections. A significant anomaly is observed on the three panels around 1750 m. Overall the total near-surface correction varies from 50 ms at the origin of the section to -50 ms on the opposite side.

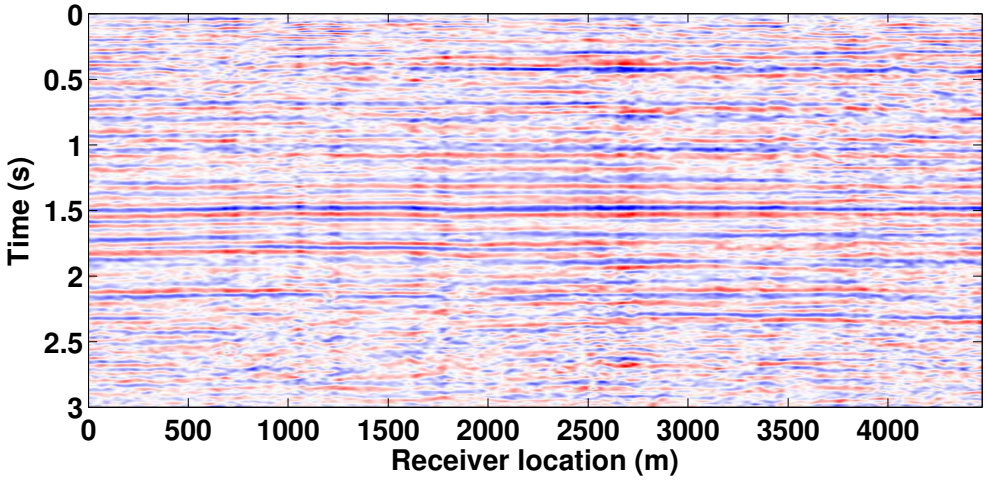

FIG. 17. Common-receiver stacked section after applying rayparameter dependent near-surface corrections. Notice how continuity and coherency of the events have been improved in comparison to Figure 12. Shallow events ($<$1 s) are now easier to identify and the undulations have been removed.

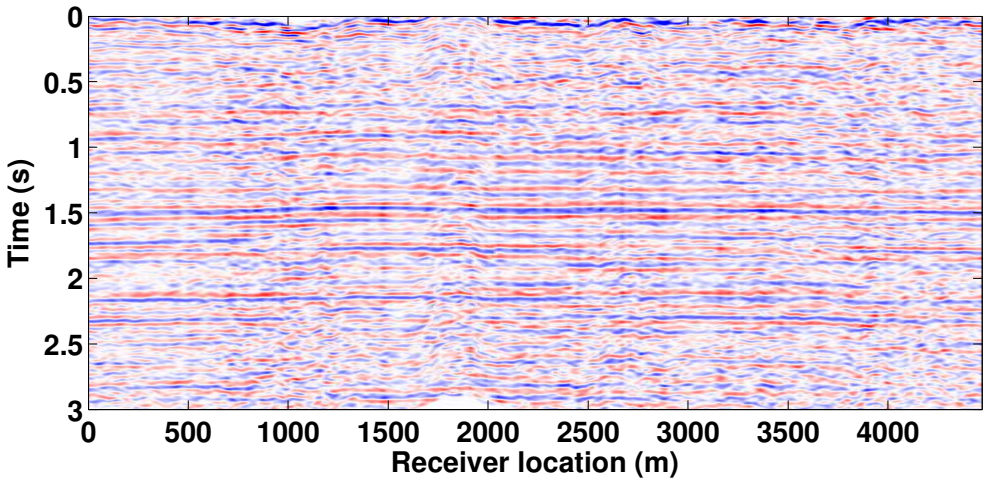

FIG. 18. Common-receiver stacked section after applying surface-consistent static corrections. Though the undulations and shifts have been removed the coherency and stack power of shallow events is poor.

very low misfit values ($\sim$ 4 ms) for the receivers nearby the reference location. However, these misfit levels could not be reached at any other location along the line. This implies that more than one reference locations might be needed to obtain a better calibration along larger seismic lines.

Even though the field data processing shown here considered a two-layered velocity model, the physical framework presented earlier allows for models with several layers. The extension of this approach into a tomographic solution is also possible and this application remains to be explored.

ACKNOWLEDGMENTS

The authors thank the sponsors of CREWES for continued support. This work was funded by CREWES industrial sponsors and NSERC (Natural Science and Engineering Research Council of Canada) through the grant CRDPJ 461179-13.

REFERENCES

Askari, R., DeMeersman, K., and Ferguson, R. J., 2012, Estimation of near surface shear wave velocity using cmp cross-correlation of surface waves (CCSW): SEG Technical Program Expanded Abstracts 2012, 1–5.

Bessonova, E. N., Fishman, V. M., Ryaboyi, V. Z., and Sitnikova, G. A., 1974, The tau method for inversion of travel times-I. Deep seismic sounding data: Geophysical Journal of the Royal Astronomical Society, **36**, No. 2, 377–398.

Claerbout, J. F., 1983, Ground roll and radial traces: Stanford Expl. Project Report, **SEP-35**, 43–53.

Cova, R., Henley, D., Wei, X., and Innanen, K. A., 2017, Receiver-side near-surface corrections in the τ-p domain: A raypath-consistent solution for converted wave processing: Geophysics, **82**, No. 2, U13–U23.

Cox, M., 1999, Static Corrections for Seismic Reflection Surveys, Geophysical references; v. 9: Society of Exploration Geophysicists.

Diebold, J. B., and Stoffa, P. L., 1981, The traveltime equation, tau-p mapping, and inversion of common midpoint data: Geophysics, **46**, No. 3, 238–254.

Eaton, D. W. S., Cary, P. W., and Schafer, A. W., 1991, Estimation of P-SV statics using stack-power optimization: CREWES Research Report, **3**, 32.1–32.18.

Garotta, R., and Granger, P. Y., 1988, Acquisition and processing of 3C $\times$ 3-D data using converted waves: SEG Technical Program Expanded Abstracts 1988, 995–997.

Hake, H., 1986, Slant stacking and its significance for anisotropy: Geophysical Prospecting, **34**, No. 4, 595–608.

Henley, D., 2012, Interferometric application of static corrections: Geophysics, **77**, No. 1, Q1–Q13.

Henley, D. C., 2014, Raypath interferometry vs. conventional statics: Recent field data and model comparisons: SEG Technical Program Expanded Abstracts 2014, 2040–2044.

Margrave, G., Bertram, M., Bertram, K., Hall, K., Innanen, K., Lawton, D., Mewhort, L., and Phillips, T., 2012, A low-frequency seismic field experiment: SEG Technical Program Expanded Abstracts 2012, 1–5.

Operto, S., Gholami, Y., Prieux, V., Ribodetti, A., Brossier, R., Metivier, L., and Virieux, J., 2013, A guided tour of multiparameter full-waveform inversion with multicomponent data: From theory to practice, **32**, No. 9, 1040–1054.

Qu, Y., Li, Z., Huang, J., Li, J., and Guan, Z., 2017, Elastic full-waveform inversion for surface topography: Geophysics, **82**, No. 5, R269–R285.

Schafer, A. W., 1991, Converted-wave statics methods comparison: CREWES Research Report, **3**, 8.107–8.125.

Virieux, J., and Operto, S., 2009, An overview of full-waveform inversion in exploration geophysics: Geophysics, **74**, No. 6, WCC1–WCC26.

Yilmaz, O., 2015, Engineering Seismology with Applications to Geotechnical Engineering:, Investigations in Geophysics: Society of Exploration Geophysicists.